Article

Gelatin-Coated High-Sensitivity Microwave Sensor for Humidity-Sensing Applications

Junho Yeo [1,*] and Younghwan Kwon [2]

1 Department of Artificial Intelligence, Daegu University, 201 Daegudae-ro, Gyeongsan-si 38453, Republic of Korea
2 Department of Energy System Engineering, Daegu University, 201 Daegudae-ro, Gyeongsan-si 38453, Republic of Korea; y_kwon@daegu.ac.kr
* Correspondence: jyeo@daegu.ac.kr; Tel.: +82-53-850-6642

Abstract: In this paper, the humidity-sensing characteristics of gelatin were compared with those of poly(vinyl alcohol) (PVA) at L-band (1 ~ 2 GHz) microwave frequencies. A capacitive microwave sensor based on a defected ground structure with a modified interdigital capacitor (DGS-MIDC) in a microstrip transmission line operating at 1.5 GHz without any coating was used. Gelatin is a natural polymer based on protein sourced from animal collagen, whereas PVA is a high-sensitivity hydrophilic polymer that is widely used for humidity sensors and has a good film-forming property. Two DGS-MIDC-based microwave sensors coated with type A gelatin and PVA, respectively, with a thickness of 0.02 mm were fabricated. The percent relative frequency shift (PRFS) and percent relative magnitude shift (PRMS) based on the changes in the resonant frequency and magnitude level of the transmission coefficient for the microwave sensor were used to compare the humidity-sensing characteristics. The relative humidity (RH) was varied from 50% to 80% with a step of 10% at a fixed temperature of around 25 °C using a low-reflective temperature and humidity chamber manufactured with Styrofoam. The experiment's results show that the capacitive humidity sensitivity of the gelatin-coated microwave sensor in terms of the PRFS and PRMS was higher compared to that of the PVA-coated one. In particular, the sensitivity of the gelatin-coated microwave sensor at a low RH from 50% to 60% was much greater compared to that of the PVA-coated one. In addition, the relative permittivity of the fabricated microwave sensors coated with PVA and gelatin was extracted by using the measured PRFS and the equation was derived by curve-fitting the simulated results. The change in the extracted relative permittivity for the gelatin-coated microwave sensor was larger than that of the PVA-coated one for varying the RH.

Keywords: gelatin; polyvinyl alcohol; defected ground structure with a modified interdigital capacitor (DGS-MIDC); microwave humidity sensor; high sensitivity

1. Introduction

Humidity refers to the amount of water vapors existing in the air [1], and it is an important physical quantity that evaluates air quality along with temperature. An accurate measurement of humidity is necessary because human quality of life, human health, and the environment, as well as products and processes in various industrial fields are significantly affected by humidity along with temperature [2]. Two commonly used definitions of humidity are absolute humidity and relative humidity (RH). The RH has been widely used for humidity measurements because of RH sensors' simplicity and affordability [3]. Based on the transduction techniques or sensing methods, RH sensors can be classified as resistive, capacitive, optical, gravimetric, piezoresistive, and magnetoelastic [4]. Among the various RH measurement techniques, the electrical properties of humidity-sensing materials, such as resistance (or electrical conductivity) and capacitance, were the most commonly used [5]. Resistive-type humidity sensors are based on the change in the resistance or conductivity of the sensing material for the different RHs, whereas capacitive-type humidity sensors are

associated with the change in capacitance of the sensing material through the variations in relative permittivity. In addition, materials for resistive-type humidity sensors can be divided into low-resistance and high-resistance materials. Note that high-resistance materials are affected by both the resistance and capacitance changes, and that the humidity sensors that incorporate high-resistance materials are called impedance-type sensors.

The humidity-sensing characteristics of the RH sensors mainly depend on the microscopic structure of the material used as the humidity-sensing layer, such as the size of the pores, the uniformity of the surface morphology, or the thickness of the layer [1,2]. It is well known that materials with porous and irregular surface morphologies show a higher humidity-sensing ability because the porous and irregular surface areas provide more empty spaces for the absorption of the hydroxyl group and hydronium ions in water molecules. The RH-sensing materials can be classified as polymers, ceramics, carbon-based materials, and composite and hybrid materials.

Porous ceramics, such as metal oxides and spinel- and perovskite-type oxides, have been used for the humidity sensors [6]. Alumina (Al_2O_3)-, Zinc (Zn)-, tin (Sn)-, anatase (TiO_2, titanium oxide)-, tungsten (W)-, hematite (Fe_2O_3), and cobalt (Co_3O_4)-based oxides are commonly used to create metal oxides [7–14]. Perovskite-type ceramics, such as $BaTiO_3$, $PbTiO_3$, $CaTiO_3$, $LaFeO_3$, $ZnSnO_3$, and $NaTaO_3$, have been used in humidity sensors [15–21]. $MgAl_2O_4$, $MgFe_2O_4$, $MgCr_2O_4$-TiO_2, and $ZnCr_2O_4$-k_2CrO_4 are spinel-type ceramics used to create humidity sensors [22–25]. Oxygen-free ceramics, such as zeolites and clay materials, were also used for the humidity sensors [26,27].

Carbon-based materials, such as carbon nanotubes (CNTs), carbon nano-coils (CNCs), and graphene oxide (GO), have been widely used in humidity sensors. CNTs are seamless cylinders consisting of one or several graphene layers and can be either single-walled (SWCNTs) or multi-walled (MWCNTs) [28]. CNTs can absorb large amounts of water molecules due to their very large surface area-to-volume ratio and their porous structures when used for humidity sensors [29]. CNCs are quasi-one-dimensional materials with unique helical morphology and can provide abundant spaces for the adsorption of water molecules for humidity sensing [30]. Graphene is a two-dimensional monolayer of sp^2-bonded carbon atoms, whereas GO is a graphene derivative with carbon atoms linked to oxygen functional groups. The addition of oxygen functional groups results in GO having excellent absorption properties when used in humidity sensors [31].

Polymers have been most widely used for humidity-sensing materials because of their advantages, such as their low cost, easy fabrication process, and their good stability [32]. Polymer humidity sensors can also be categorized into the resistive type and the capacitive type. The resistive-type polymer humidity sensors are divided into the ionic-conduction type and the electronic-conduction type. The ionic-conduction polymers are polyelectrolytes, which are polymers with electrolytic groups, such as quaternary ammonium salt, sulfonate salt, and phosphonium salt [33–35]. The electronic-conduction types are conducting/semiconducting polymers such as polyaniline (PANI) [36], poly(p-diethynylbenzene) (PDEB) [37], poly(3,4-ethylenedioxythiophene) (PEDOT) [38], and poly(3,4-ethylenedioxythiophene)–poly(styrene-sulfonate) (PEDOT-PSS) [39].

Various capacitive-type polymers have been used for RH sensors due to their advantages, such as their simpler fabrication, rapid responses, small hysteresis, and their excellent stability, compared to resistive-type polymers [32]. The capacitive-type polymers are insulating polymers whose permittivity varies depending on the amount of absorbed water as a function of humidity, such as poly(methyl methacrylate) (PMMA), polyimide, poly(2-hydroxyethyl methacrylate) (PHEMA), and poly(vinyl alcohol) (PVA) [40–43]. It was reported in the literature that the humidity-sensing sensitivity of PVA is higher than polyimide, PMMA, and PHEMA [44]. Cellulose derivatives, such as cellulose acetate butyrate (CAB) or cellulose nanofibers (CNF), have also been used for capacitive humidity sensors [45].

Gelatin is a natural polymer based on protein sourced from collagen, which is mainly obtained from the skins, connective tissues (tendons and ligaments), and bones of cows

and pigs [46]. In general, gelatin can be divided into two types by using raw materials and the pre-treatment applied during the manufacturing process: type A with an acid treatment, and type B with an alkaline treatment. Recently, gelatin's humidity-sensing ability has been studied because of its hygroscopic characteristics with biocompatibility and biodegradability. The changes in the resistance of a gold interdigitated electrode (IDE) structure coated with gelatin polymer were measured when the RH varied from 15% to 86% [47]. The performance of gelatin as a capacitive humidity-sensing material was examined with the changes in the capacitance of a planar IDE coated with gelatin when the RH was ramped up and down between 50% and 90% with a step of 10% [48]. However, these characteristic studies were conducted in the low-frequency band, and a comparison of the humidity sensitivity for gelatin with other polymers using a capacitive microwave sensor has never previously been studied in microwave frequency bands (0.3 to 300 GHz). The chemical structures of PVA [49] and gelatin [50] are shown in Figure 1. PVA is a water-soluble synthetic polymer consisting of a carbon chain as its backbone, and a hydroxyl (OH) functional group, and has various desirable properties, such as a high hydrophilicity, biocompatibility, and good film-forming and process abilities [51]. Gelatin is a natural polymer with a heterogeneous mixture of single- or multi-stranded polypeptides containing between 300 and 4000 amino acids [52]. The amino acid compositions of gelatin are 26~30% of glycine (Gly), 14~18% of proline (Pro), 13~15% of hydroxyproline (Hyp), 11~12% of glutamic acid (Glu), 8~10% of alanine (Ala), 8~9% of arginine (Arg), and other amino acids [53]. The hydroxyl functional group in hydroxyproline might play an important role in the humidity-sensing capability along with the porous structure of gelatin.
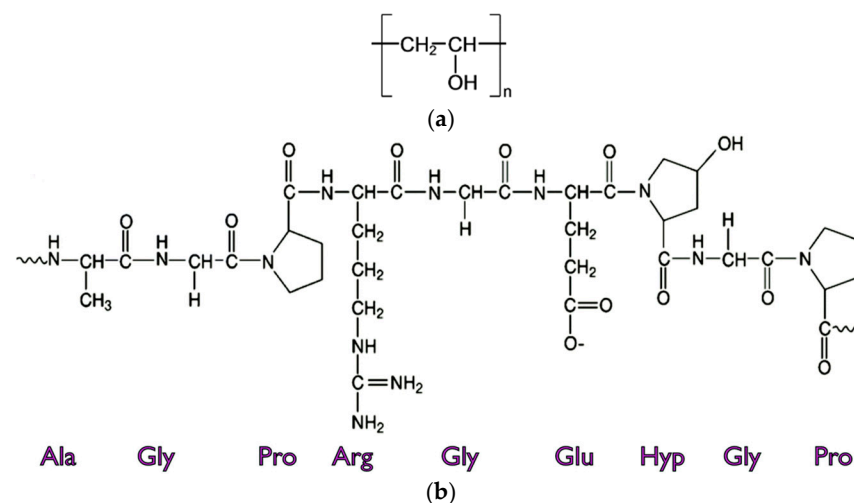

Figure 1. Chemical structures of (**a**) PVA and (**b**) gelatin.

Planar microwave technology-based sensors have been widely used because of their advantages, such as their low profile, low cost, their simple structure, and their ease of fabrication [54]. Among various methods, the resonant frequency-based methods using planar microwave resonators, such as the split-ring resonator (SRR) or the complementary SRR (CSRR), implemented on microstrip transmission lines, have been extensively used [55,56]. It was found that an interdigital-capacitor-shaped defected ground structure-based microwave sensor has a higher sensitivity for the variations in relative permittivity, compared to other microwave sensors using a single-ring, a rotated single-ring, or a double-ring CSRR [56].

In this paper, gelatin's humidity-sensing ability was compared with that of PVA at L-band (1~2 GHz) microwave frequencies. A high-sensitivity capacitive microwave sensor based on a defected ground structure with a modified interdigital capacitor (DGS-MIDC) in a microstrip transmission line resonating at 1.5 GHz without any coating was designed on an RF-301 substrate with a thickness of 0.76 mm [44]. Two microwave sensors coated

with gelatin and PVA, respectively, with a thickness of 0.02 mm were fabricated. The first resonant frequency and the magnitude level of the transmission coefficient (S_{21}) for the microwave sensors were used to compare the humidity-sensing characteristics when the RH was varied from 50% to 80% with a step of 10% at a temperature of 25 °C using a low-reflective temperature and humidity chamber manufactured with Styrofoam. All the simulated results in this paper were obtained using CST Studio Suite (Dassault Systèmes Co., Vélizy-Villacoublay, France) [57].

2. Microwave Sensor Geometry and Characteristic

A high-sensitivity two-port microwave sensor based on a DGS-MIDC was designed on a 50 mm × 50 mm RF-301 substrate with a relative permittivity (ε_r) of 2.97, a loss tangent ($\tan \delta$) of 0.0009, and a thickness of 0.76 mm to concentrate the electric field along the microstrip transmission line, as shown in Figure 2a. The DGS-MIDC was etched on the ground plane of the microstrip transmission line with a width of 1.68 mm, and the geometric parameters were optimized to obtain the first resonant frequency of S_{21} at 1.5 GHz for unloaded conditions with a high sensitivity for relative permittivity. The proposed microwave sensor with the DGS-MIDC showed a band-stop characteristic at the resonant frequencies. When a capacitive polymer is coated on the top of the DGS-MIDC, the resonant frequencies of the microwave sensor change according to the variations in complex permittivity of the coated capacitive polymer for different RHs.
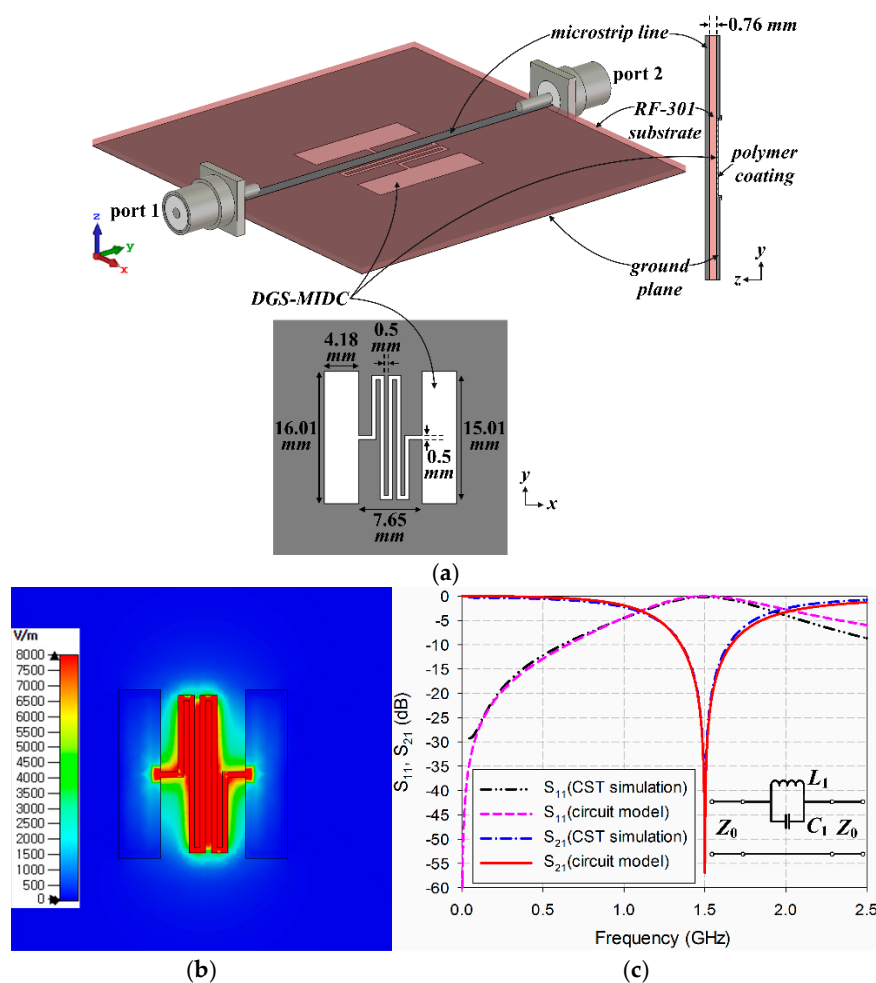

Figure 2. DGS-MIDC-based microwave sensor: (**a**) geometry, (**b**) electric-field distribution at 1.5 GHz, and (**c**) S-parameter characteristics and simplified equivalent circuit model.

We note that the polymer-coated square area's length was 18.01 mm, slightly longer than that of the DGS-MIDC, providing complete coverage, and the thickness of the coated area was measured to be 0.02 mm. The electric-field distributions were mainly concentrated along the slots between the interdigital fingers, as shown in Figure 2b. The simplified equivalent circuit model of the proposed IDCS-DGS considering only the first resonant frequency is shown as the inset in Figure 2c, and the circuit parameters can be obtained from the CST Studio Suite simulation results by using the following equations [58]:

$$C_1 = \frac{1}{Z_0} \frac{1}{4\pi \Delta f_{3dB}} \tag{1}$$

$$L_1 = \frac{1}{(2\pi f_r)^2 C_1} \tag{2}$$

where Z_0 is the characteristic impedance of the transmission line, f_r is the resonant frequency, and Δf_{3dB} is the 3 dB bandwidth at the first resonant frequency. The extracted circuit parameters for unloaded conditions are C_1 = 1.6938 pF and L_1 = 6.6464 nH, and the S-parameters obtained from these circuit parameters were compared with the simulation results in Figure 2c, which showed good agreement.

The changes in the first resonant frequency (f_r) and the percent relative frequency shift (PRFS) of the S_{21} characteristics for the microwave sensor with the DGS-MIDC are shown in Figure 3. The PRFS is a percentage of the difference between the loaded and unloaded first resonant frequencies compared to the unloaded first resonant frequency. The coated polymer's relative permittivity (ε_r) changed from 1 to 24 for the lossless case (tan δ = 0) [44]. As the relative permittivity increased, the first resonant frequency decreased. For example, the first resonant frequency moved to 1.3793 GHz and its PRFS compared to the unloaded one at 1.5 GHz was 8.05% when the relative permittivity increased from 1 to 24.
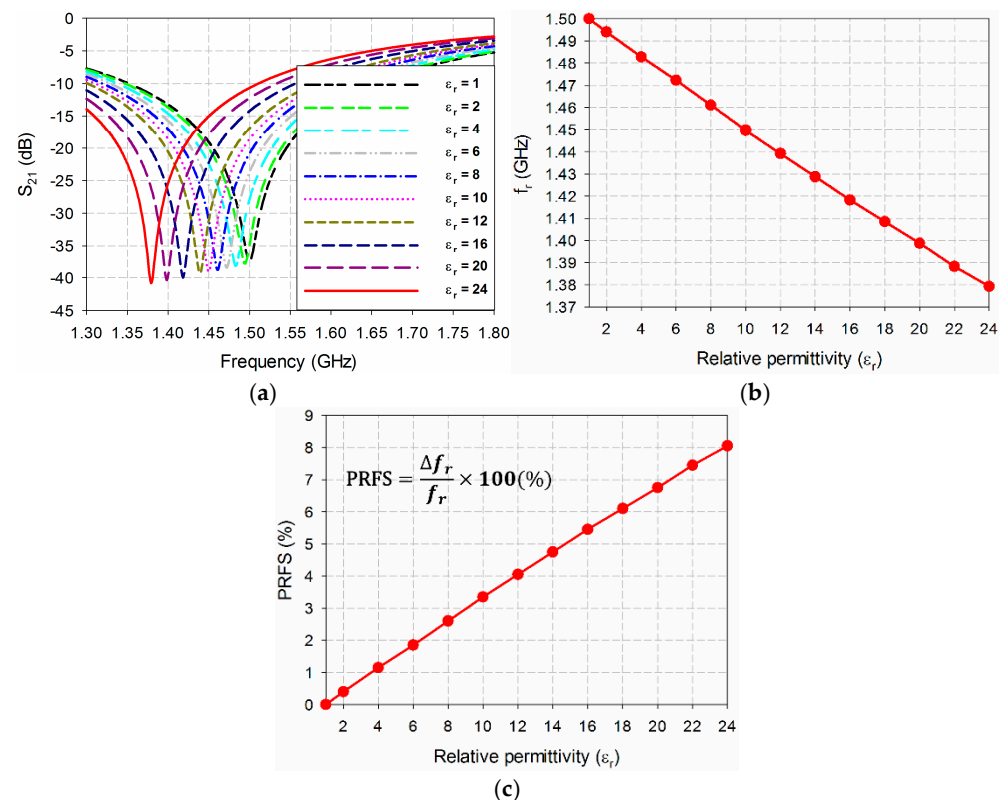

Figure 3. Performance characteristics of the DGS-MIDC-based microwave sensor for varying relative permittivity of the coated polymer with tan δ = 0: (**a**) S_{21}, (**b**) f_r, and (**c**) PRFS.

Table 1 summarizes the simulated values of the first resonant frequencies and PRFSs for the different relative permittivities varying from 1 to 24.

Table 1. First resonant frequencies and PRFS of S_{21} responses of the DGS-MIDC-based microwave sensor for varying relative permittivity of the coated polymer with tan $\delta = 0$.

	$\varepsilon_r = 1$	$\varepsilon_r = 2$	$\varepsilon_r = 4$	$\varepsilon_r = 6$	$\varepsilon_r = 8$	$\varepsilon_r = 10$	$\varepsilon_r = 12$	$\varepsilon_r = 14$	$\varepsilon_r = 16$	$\varepsilon_r = 18$	$\varepsilon_r = 20$	$\varepsilon_r = 22$	$\varepsilon_r = 24$
f_r (GHz)	1.5	1.4940	1.4828	1.4723	1.4610	1.4497	1.4393	1.4288	1.4183	1.4085	1.3987	1.3883	1.3793
PRFS (%)	0	0	0.40	1.15	1.85	2.60	3.35	4.05	4.75	5.45	6.10	6.75	7.45	8.05

It turned out that the variation in the PRFS in the first resonant frequency of S_{21} showed a nearly linear behavior for the varying relative permittivity from 1 to 24. Based on this knowledge, the relation of relative permittivity in terms of the PRFS was derived from a curve-fitting tool in Sigma Plot by using the following equation:

$$\varepsilon_r = A_0 + A_1 \times PRFS + A_2 \times (PRFS)^2 \tag{3}$$

where $A_0 = 1.0075$, $A_1 = 2.5825$, and $A_2 = 0.0331$.

Figure 4 shows the extracted equivalent capacitance and inductance, and their percent relative shifts when the relative permittivity of the MUT polymers varies from 1 to 24 with tan $\delta = 0$. In this case, both the equivalent capacitance and inductance changed linearly. For instance, when the relative permittivity of the MUT was $\varepsilon_r = 1$, C_1 and L_1 of the proposed microwave sensor were 1.6938 pF and 6.6464 nH, respectively. As the relative permittivity of the MUT increased to $\varepsilon_r = 24$, C_1 and L_1 were increased to 1.9541 pF and 6.8141 nH, respectively. Therefore, $\Delta C_1 / C_1 (\%)$ and $\Delta L_1 / L_1 (\%)$ were 15.4% and 2.5%, respectively. Both C_1 and L_1 show nearly linear behaviors, but the variation in C_1 is much higher compared to L_1.
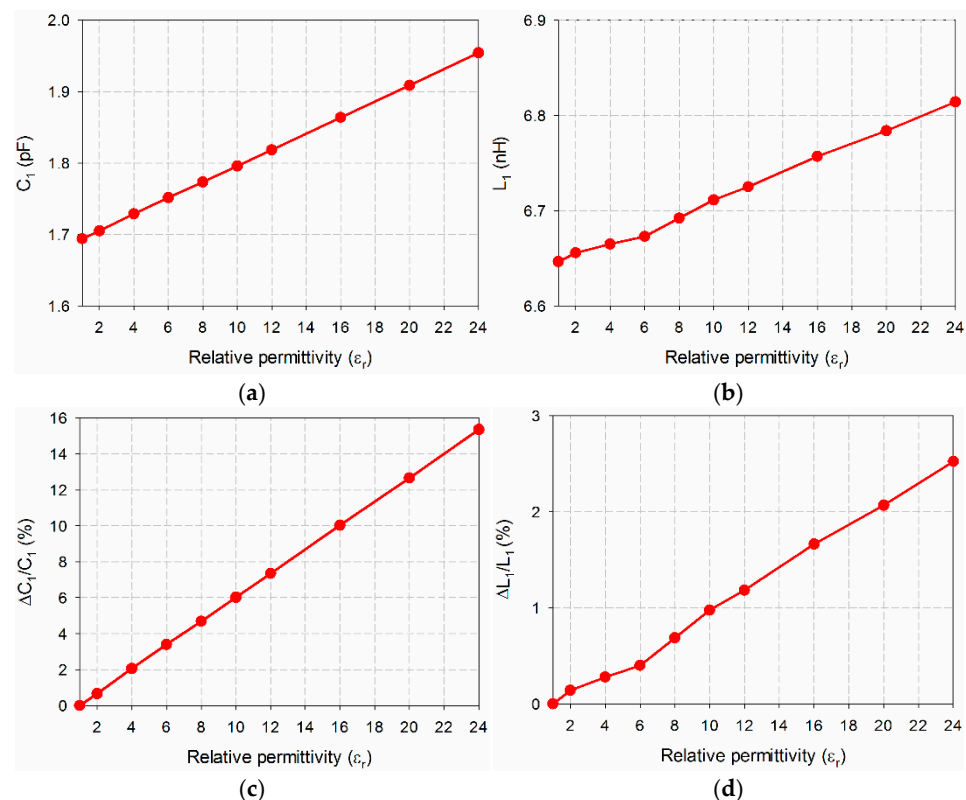

Figure 4. Extracted equivalent circuit parameters of the DGS-MIDC-based microwave sensor for varying relative permittivity of the coated polymer with tan $\delta = 0$: (**a**) C_1; (**b**) L_1; (**c**) $\Delta C_1 / C_1 (\%)$ and (**d**) $\Delta L_1 / L_1 (\%)$.

3. Experiment Results and Discussion

Figure 5a,b shows photographs of the microwave sensors based on the DGS-MIDC coated with PVA and gelatin, respectively, fabricated on an RF-301 substrate. The PVA with a degree of polymerization of 1500 and a degree of saponification of 99 mol% was obtained from Yakuri Pure Chemicals Co., Ltd., Kyoto, Japan, whereas the type A gelatin (G1890-100G, gel strength ~300 g Bloom, from porcine skin) was provided by Sigma-Aldrich Co., St. Louis, MO, USA. The preparation of the polymer solutions with a concentration of 5 wt% was carried out by dissolving each polymer using deionized water as a solvent. First, each polymer solution of 55 mg was spread over the sensing area on the DGS-MIDC using a brush. Next, a convection oven (OF4-10P, JEIO TECH Co., Ltd., Daejeon, Republic of Korea) was used to dry the polymer-coated microwave sensors for 120 min at 60 °C. Finally, overnight drying in a vacuum oven (JSOV-30T, JS Research Inc., Gongju, Republic of Korea) was carried out at 80 °C. Field-emission scanning electron microscopy (S-4300, Hitachi High-Technologies Co., Ltd., Tokyo, Japan) was used at a voltage of 15 kV to measure the average thickness of the coated polymer film, and it was around 0.02 mm.
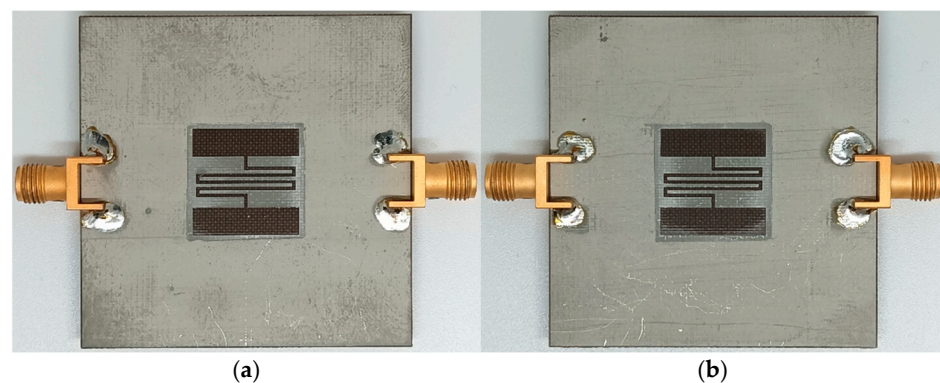

(**a**)   (**b**)

Figure 5. Photographs of the fabricated microwave sensors coated with (**a**) PVA and (**b**) gelatin.

For the humidity-sensing measurements, the experimental setup shown in Figure 6 was used. A custom-made low-reflective temperature and humidity chamber was manufactured using 50 mm thick Styrofoam walls, a thermostat for controlling temperature, a humidistat for controlling humidity, halogen lamps for adding temperature, and a humidifier for adding humidity. The MegiQ VNA-0460 (MegiQ, Eindhoven, The Netherlands) vector network analyzer was used to measure the S_{21} characteristics of the polymer-coated fabricated microwave sensors. The RH was increased from 50% to 80% with a step of 10% with a fixed temperature of around 25 °C. For the stabilization of the humidity inside the chamber along with ensuring water absorption into the polymer-coated area, the S_{21} characteristics were measured after waiting 10 min for each RH.

The measured S_{21} characteristics of the fabricated microwave humidity sensors coated with PVA and gelatin, respectively, for each RH were compared in Figure 7. The measured first resonant frequency and magnitude level of the fabricated microwave sensors without a polymer coating (unloaded conditions) were 1.526 GHz and −37.38 dB, respectively. When the RH increased from 50% to 80% for the PVA-coated microwave sensor, the S_{21}'s first resonant frequency moved from 1.496 GHz to 1.446 GHz, while its magnitude level increased from −33.69 dB to −27.79 dB. As the RH increased from 50% to 80% for the gelatin-coated microwave sensor, the S_{21}'s first resonant frequency shifted from 1.478 GHz to 1.419 GHz, while its magnitude level increased from −32.82 dB to −24.41 dB. The values of the measured first resonant frequencies, PRFSs, magnitude levels, and percent relative magnitude shifts (PRMSs) of the fabricated microwave humidity sensors coated with PVA and gelatin are summarized in Tables 2 and 3. Note that the PRMS is a percentage of the difference between the magnitude levels at the loaded and unloaded first resonant frequencies compared to the magnitude level at the unloaded first resonant frequency [44].
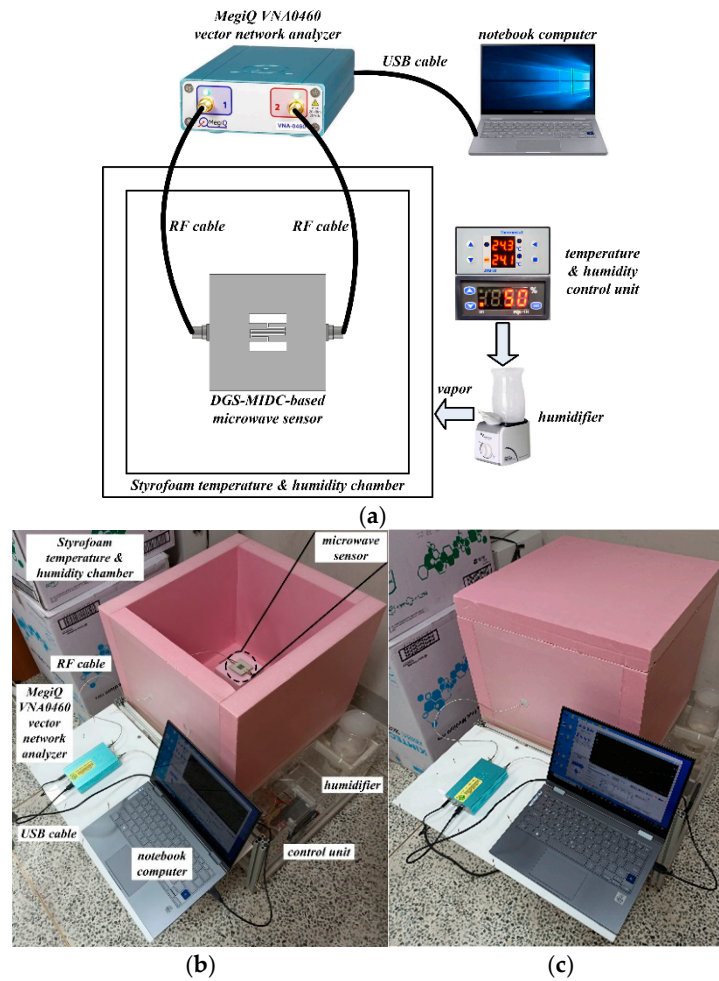
(a)

(b)   (c)

Figure 6. Block diagram and photographs of the experiment setup for the humidity-sensing measurements: (**a**) block diagram, (**b**) experiment setup with an open-top cover, and (**c**) experiment setup with closed-top cover.

(a)   (b)
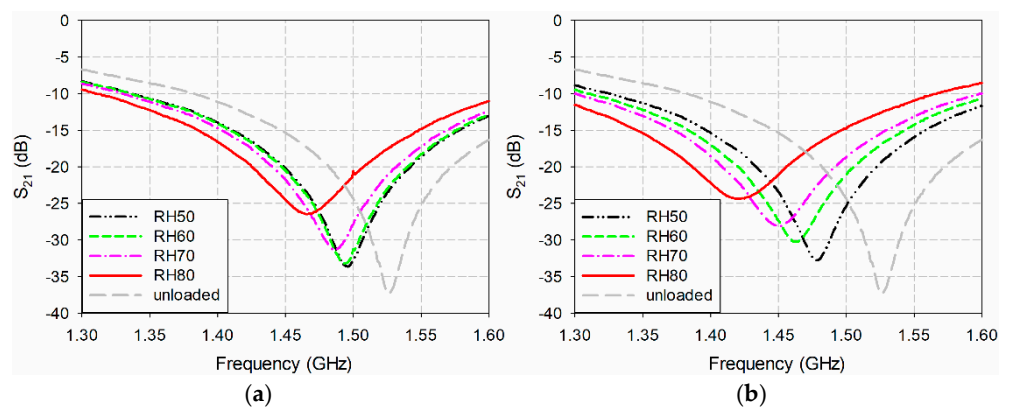
Figure 7. Measured S_{21} characteristics of the fabricated microwave sensors coated with the polymers for varying RH. (**a**) PVA and (**b**) gelatin.

Figure 8 shows a plot of the measured first resonant frequencies, PRFSs, magnitude levels, and PRMSs of the fabricated microwave sensors coated with PVA and gelatin as a function of the RH, which are obtained from the results in Figure 7. The inset in Figure 8d shows the definition of PRMS. The PRFSs and PRMSs were calculated based on the first resonant frequency and magnitude level of the fabricated microwave sensor without any coating. When the RH increased from 50% to 80% for the PVA-coated microwave sensor, the

PRFS increased 2.0 times from 1.97% to 3.93%, while the PRMS increased 2.59 times from 9.89% to 25.66%. As the RH increased from 50% to 80% for the gelatin-coated microwave sensor, the PRFS increased 2.23 times from 3.15% to 7.01%, while the PRMS increased 2.84 times from 12.21% to 34.71%. Accordingly, the capacitive humidity sensitivity of the gelatin-coated microwave sensor is higher compared to that of the PVA-coated one in terms of the PRFS and PRMS.

Table 2. Measured first resonant frequencies, PRFSs, magnitude levels, and PRMSs of S_{21} responses of the DGS-MIDC-based microwave sensor coated with PVA for varying RH.

PVA	Unloaded	RH50	RH60	RH70	RH80
f_r (GHz)	1.526	1.496	1.493	1.487	1.466
PRFS (%)	0	1.97	2.16	2.56	3.93
S_{21} (dB)	−37.38	−33.69	−33.24	−31.36	−27.79
PRMS (%)	0	9.89	11.09	16.12	25.66

Table 3. Measured first resonant frequencies, PRFSs, magnitude levels, and PRMSs of S_{21} responses of the DGS-MIDC-based microwave sensor coated with gelatin for varying RH.

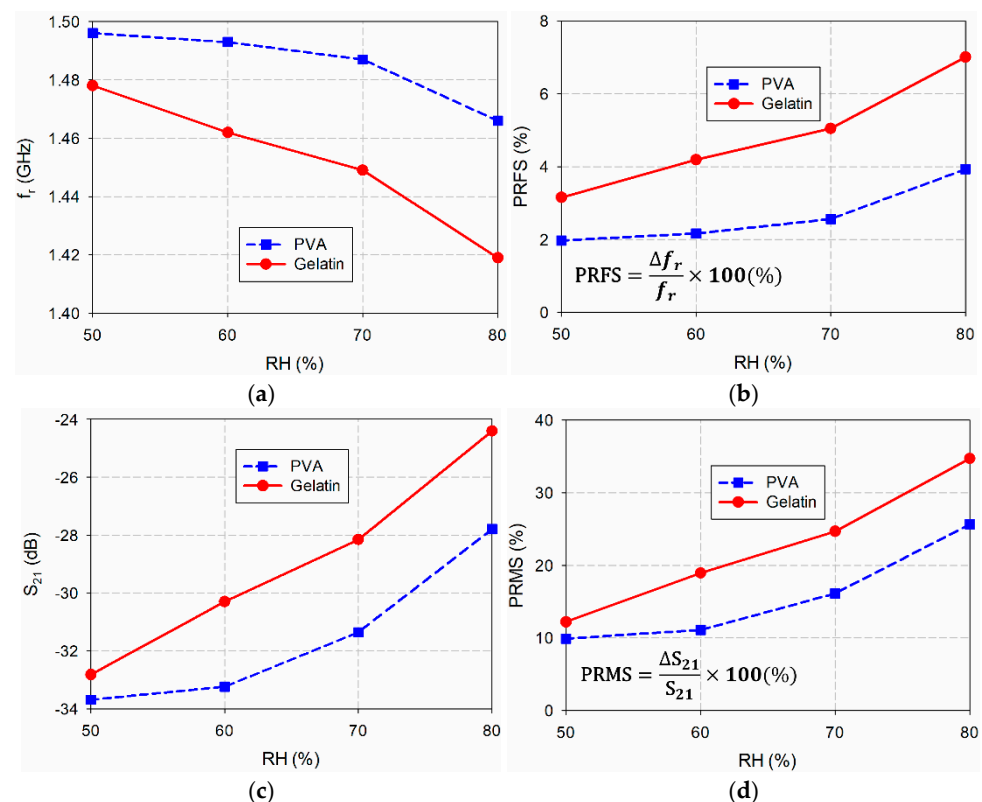| Gelatin	Unloaded	RH50	RH60	RH70	RH80
f_r (GHz)	1.526	1.478	1.462	1.449	1.419
PRFS (%)	0	3.15	4.19	5.05	7.01
S_{21} (dB)	−37.38	−32.82	−30.30	−28.15	−24.41
PRMS (%)	0	12.21	18.95	24.69	34.71

Figure 8. Performance comparison of the fabricated microwave sensors coated with the polymers for varying RH. (**a**) f_r, (**b**) PRFS, (**c**) S_{21} magnitude, and (**d**) PRMS.

Finally, the relative permittivity of the fabricated sensors coated with PVA and gelatin was extracted by using the measured PRFSs and Equation (3), as shown in Figure 9. When the RH increased from 50% to 80% for the PVA-coated microwave sensor, the relative

permittivity increased 1.88 times from 6.22 to 11.67, while it increased 2.19 times from 9.47 to 20.74 for the gelatin-coated sensor. Note that the relative permittivity of PVA at around 1.5 GHz is around 4 to 5 [59], whereas that of gelatin is around 7 to 8 [60]. The relative permittivity of the PVA film for varying the RH can also be calculated by using equations in [61]. It increased 1.89 times from 5.87 to 11.09 when the RH increased from 50% to 80%, which shows a similar trend with slightly smaller values compared to that derived from equation (3). Therefore, we can conclude that the change in the extracted relative permittivity for the gelatin-coated microwave sensor is larger than that of the PVA-coated one for the varying RH.
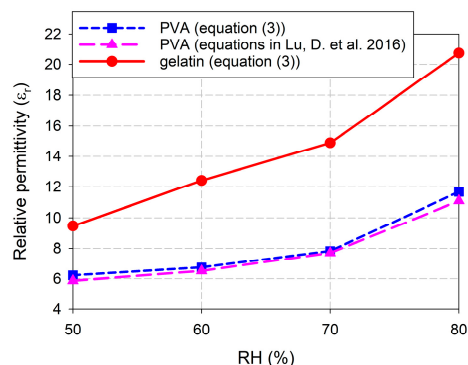

Figure 9. Comparison of the extracted relative permittivity from measured PRFSs of PVA- and gelatin-coated microwave sensors for varying RH.

4. Conclusions

We have compared the capacitive humidity-sensing performance of gelatin and PVA polymers using a planar microwave sensor based on a DGS-MIDC with a first band-stop frequency at 1.5 GHz without any coating. The variations in the first resonant frequency and the PRFS of the S_{21} characteristics were studied through a simulation when the coated polymer's relative permittivity changed from 1 to 24 for the lossless case (tan δ = 0). The quadratic relationship between the coated polymer's relative permittivity and the PRFS of the first resonant frequency was derived by using a curve fitting tool.

The prototypes of the microwave sensors coated with type A gelatin and PVA, respectively, with a thickness of 0.02 mm, were fabricated on an RF-301 substrate. When the RH was varied from 50% to 80% with a step of 10% at a temperature of 25 °C, the humidity-sensing characteristics of the gelatin- and PVA-coated microwave sensors were compared by using the changes in the resonant frequency and magnitude level of S21. For the PVA-coated microwave sensor, the PRFS increased 2.0 times from 1.97% to 3.93% when the RH increased from 50% to 80%, whereas it increased 2.23 times from 3.15% to 7.01% for the gelatin-coated microwave sensor. The PRMS increased 2.59 times from 9.89% to 25.66% as the RH increased from 50% to 80% for the PVA-coated microwave sensor, whereas it increased 2.84 times from 12.21% to 34.71% for the gelatin-coated microwave sensor. Therefore, the sensitivities of the gelatin-coated microwave sensor in terms of the PRFS and PRMS are higher compared to those of the PVA-coated microwave sensor.

A similar trend was observed in the variations of the extracted relative permittivity based on the measured PRFSs. For the PVA-coated microwave sensor, the extracted relative permittivity increased 1.88 times from 6.22 to 11.67 when the RH increased from 50% to 80%, whereas it increased 2.19 times from 9.47 to 20.74 with a larger change for the gelatin-coated sensor.

Therefore, gelatin can be a potential candidate for a high-sensitivity natural capacitive humidity-sensing material to replace PVA for various microwave sensors, such as chipless RFID tags, wireless sensors, or wearable sensors. The mechanical, physical, and chemical stability, repeatability, and reliability of gelatin and PVA need to be explored further in

future work. We also plan to compare the humidity-sensing performances between type A and type B gelatins.

References

1. Sajid, M.; Khattak, Z.; Rahman, K.; Hassan, G.; Choi, K.H. Progress and future of relative humidity sensors: A review from materials perspective. *Bull. Mater. Sci.* **2022**, *45*, 238. [CrossRef]
2. Arman Kuzubasoglu, B. Recent studies on the humidity sensor: A mini review. *ACS Appl. Electron. Mater.* **2022**, *4*, 4797–4807. [CrossRef]
3. Farahani, H.; Wagiran, R.; Hamidon, M.N. Humidity sensors principle, mechanism, and fabrication technologies: A comprehensive review. *Sensors* **2014**, *14*, 7881–7939. [CrossRef] [PubMed]
4. Lee, C.Y.; Lee, G.B. Humidity sensors: A review. *Sens. Lett.* **2005**, *3*, 1–15. [CrossRef]
5. Ali, S.; Hassan, A.; Hassan, G.; Bae, L.; Lee, C. All-printed humidity sensor based on graphene/methyl-red composite with high sensitivity. *Carbon* **2016**, *105*, 23–32. [CrossRef]
6. Blank, T.A.; Eksperiandova, L.P.; Belikov, K.N. Recent trends of ceramic humidity sensors development: A review. *Sens. Actuators B Chem.* **2016**, *228*, 416–442. [CrossRef]
7. Sekulić, D.L.; Ivetić, T.B. Characterization of an impedance-type humidity sensor based on porous SnO_2/TiO_2 composite ceramics modified with molybdenum and zinc. *Sensors* **2023**, *23*, 8261. [CrossRef] [PubMed]
8. Pan, S.; Gayathri, G.; Reshma, T.S.; Mangamma, G.; Prasad, A.K.; Das, A. A sensitive humidity sensor at low pressure with SnO_2 QDs. *Sens. Actuators A-Phys.* **2022**, *346*, 113835. [CrossRef]
9. Li, H.; Meng, B.; Jia, H.; Wang, D.; Wei, Z.; Li, R.; Chen, R. Optical humidity sensor based on ZnO nanomaterials. In Proceedings of the 2020 IEEE 5th Optoelectronics Global Conference (OGC), Shenzhen, China, 7–11 September 2020; pp. 169–172.
10. Li, F.; Li, P.; Zhang, H. Preparation and research of a high-performance ZnO/SnO_2 humidity sensor. *Sensors* **2022**, *22*, 293. [CrossRef]
11. Sun, L.; Haidry, A.A.; Fatima, Q.; Li, Z.; Yao, Z. Improving the humidity sensing below 30% RH of TiO_2 with GO modification. *Mater. Res. Bull.* **2018**, *99*, 124–131. [CrossRef]
12. Wang, Z.; Fan, X.; Li, C.; Men, G.; Han, D.; Gu, F. Humidity-sensing performance of 3DOM WO_3 with controllable structural modification. *ACS Appl. Mater. Interfaces* **2018**, *10*, 3776–3783. [CrossRef] [PubMed]
13. Khan, M.U.; Hassan, G.; Awais, M.; Bae, J. All printed full range humidity sensor based on Fe_2O_3. *Sens. Actuators A Phys.* **2022**, *311*, 112072. [CrossRef]
14. Abid, H.N.; Nayef, U.M.; Mutlak, F.A.H. Preparation and characterization Co_3O_4 nanoparticles on porous silicon for humidity sensor by photoluminescence. *Optik* **2019**, *178*, 379–383. [CrossRef]
15. He, Y.; Zhang, T.; Zheng, W.; Wang, R.; Liu, X.; Xia, Y.; Zhao, J. Humidity sensing properties of $BaTiO_3$ nanofiber prepared via electrospinning. *Sens. Actuators B Chem.* **2010**, *146*, 98–102. [CrossRef]
16. Mahmoud, A.E.; Viola, G.; Afify, A.S.; Babeer, A.M.; Ferrari, M. Processing, structural and humidity sensing properties of $PbTiO_3$ ceramic synthesized by solid state reaction. *J. Porous Mater.* **2020**, *27*, 947–958. [CrossRef]
17. Chang, D.A.; Tseng, T.Y. Humidity-sensitivity characteristics of $CaTiO_3$ porous ceramics. *J. Mater. Sci. Lett.* **1990**, *9*, 943–944. [CrossRef]
18. Zhao, J.; Liu, Y.; Li, X.; Lu, G.; You, L.; Liang, X.; Liu, F.; Zhang, T.; Du, Y. Highly sensitive humidity sensor based on high surface area mesoporous $LaFeO_3$ prepared by a nanocasting route. *Sens. Actuators B Chem.* **2013**, *181*, 802–809. [CrossRef]
19. Bauskar, D.; Kale, B.B.; Patil, P. Synthesis and humidity sensing properties of $ZnSnO_3$ cubic crystallites. *Sens. Actuators B Chem.* **2012**, *161*, 396–400. [CrossRef]
20. Zhang, Y.; Chen, Y.; Zhang, Y.; Cheng, X.; Feng, C.; Chen, L.; Zhou, J.; Ruan, S. A novel humidity sensor based on $NaTaO_3$ nanocrystalline. *Sens. Actuators B Chem.* **2012**, *174*, 485–489. [CrossRef]
21. Tambwe, K.; Ross, N.; Baker, P.; Bui, T.-T.; Goubard, F. Humidity sensing applications of lead-free halide perovskite nanomaterials. *Materials* **2022**, *15*, 4146. [CrossRef]
22. Ahn, K.; Wessels, W.B.; Sampath, S. Spinel humidity sensors prepared by thermal spray direct writing. *Sens. Actuators B Chem.* **2005**, *107*, 342–346. [CrossRef]

23. Shah, J.; Kotnala, R.K. Humidity sensing exclusively by physisorption of water vapors on magnesium ferrite. *Sens. Actuators B Chem.* **2012**, *171–172*, 832–837. [CrossRef]

24. Saha, D.; Giri, R.; Mistry, K.K.; Sengupta, K. Magnesium chromate–TiO_2 spinel tape cast thick film as humidity sensor. *Sens. Actuators B Chem.* **2005**, *107*, 323–331. [CrossRef]

25. Bayhan, M.; Kavasoglu, N. A study on the humidity sensing properties of $ZnCr_2O_4$–K_2CrO_4 ionic conductive ceramic sensor. *Sens. Actuators B Chem.* **2006**, *117*, 261–265. [CrossRef]

26. Urbiztondo, M.; Pellejero, I.; Rodriguez, A.; Pina, M.P.; Santamaria, J. Zeolite-coated interdigital capacitors for humidity sensing. *Sens. Actuators B Chem.* **2011**, *157*, 450–459. [CrossRef]

27. Prasad, N.V.K.; Prasad, K.V.; Ramesh, S.; Phanidhar, S.V.; Ratnam, K.V.; Janardhan, S.; Manjunatha, H.; Sarma, M.S.S.R.K.N.; Srinivas, K. Ceramic sensors: A mini-review of their applications. *Front. Mater.* **2020**, *7*, 593342.

28. Tulliani, J.M.; Inserra, B.; Ziegler, D. Carbon-based materials for humidity sensing: A short review. *Micromachines* **2019**, *10*, 232. [CrossRef] [PubMed]

29. Cao, C.L.; Hu, C.G.; Fang, L.; Wang, S.X.; Tian, Y.S.; Pan, C.Y. Humidity sensor based on multi-walled carbon nanotube thin films. *J. Nanomater.* **2011**, *2011*, 707303. [CrossRef]

30. Zhao, S.; Li, Y.; Wu, F.; Hu, R.; Deng, C. Humidity response of single carbon nanocoil and its temperature sensor independent of humidity and strain. *Appl. Surf. Sci.* **2022**, *605*, 154745. [CrossRef]

31. Bi, H.; Yin, K.; Xie, X.; Ji, J.; Wan, S.; Sun, L.; Terrones, M.; Dresselhaus, M.S. Ultrahigh humidity sensitivity of graphene oxide. *Sci. Rep.* **2013**, *3*, 2714. [CrossRef]

32. Chen, Z.; Lu, C. Humidity sensors: A review of materials and mechanisms. *Sens. Lett.* **2005**, *3*, 274–295. [CrossRef]

33. Lee, C.-W.; Rhee, H.-W.; Gong, M.-S. Humidity sensor using epoxy resin containing quaternary ammonium salts. *Sens. Actuators B Chem.* **2001**, *73*, 124–129. [CrossRef]

34. Sakai, Y.; Matsuguchi, M.; Yonesato, N. Humidity sensor based on alkali salts of poly(2-acrylamido-2-methylpropane sulfonic acid). *Electrochim. Acta* **2001**, *46*, 1509–1514. [CrossRef]

35. Gong, M.-S.; Lee, C.-W.; Joo, S.-W.; Choi, B.-K. Humidity-sensitive properties of phosphonium salt-containing polyelectrolytes. *J. Mater. Sci.* **2002**, *37*, 4615–4620. [CrossRef]

36. Nechtschein, M.; Santier, C.; Travers, J.P.; Chroboczek, J.; Alix, A.; Ripert, M. Water effects in polyaniline: NMR and transport properties. *Synth. Met.* **1987**, *18*, 311–316. [CrossRef]

37. Yang, M.; Li, Y.; Zhan, X.; Ling, M. A novel resistive-type humidity sensor based on poly(p-diethynylbenzene). *J. Appl. Polym. Sci.* **1999**, *74*, 2010–2015. [CrossRef]

38. Liu, J.; Agarwal, M.; Varahramyan, K.; Berney, E.S.; Hodo, W.D. Polymer-based microsensor for soil moisture measurement. *Sens. Actuators B Chem.* **2008**, *129*, 599–604. [CrossRef]

39. Skabara, P.J.; Li, L.; Vilela, F.; Uttamchandani, D.; Forgie, J. Miniature humidity micro-sensor based on organic conductive polymer—Poly(3,4-ethylenedioxythiophene). *Micro Nano Lett.* **2009**, *4*, 84–87.

40. Roman, C.; Bodea, O.; Prodan, N.; Levi, A.; Cordos, E.; Manoviciu, I. A capacitive-type humidity sensor using crosslinked poly(methylmethacrylate-co-(2 hydroxypropyl)-methacrylate). *Sens Actuators B Chem.* **1995**, *25*, 710–713. [CrossRef]

41. Boudaden, J.; Steinmaßl, M.; Endres, H.E.; Drost, A.; Eisele, I.; Kutter, C.; Müller-Buschbaum, P. Polyimide-based capacitive humidity sensor. *Sensors* **2018**, *18*, 1516. [CrossRef]

42. Reddy, A.S.G.; Narakathu, B.B.; Atashbar, M.Z.; Rebros, M.; Rebrosova, E.; Joyce, M.K. Fully printed flexible humidity sensor. *Procedia Eng.* **2011**, *25*, 120–123. [CrossRef]

43. Amin, E.M.; Karmakar, N.C.; Winther-Jensen, B. Polyvinyl-alcohol (PVA)-based RF humidity sensor in microwave frequency. *Prog. Electromagn. Res. B* **2013**, *54*, 149–166. [CrossRef]

44. Yeo, J.; Kwon, Y. Humidity sensing performance of defected ground structure-based microwave sensors coated with PMMA, PHEMA, and PVA. *Microw. Opt. Technol. Lett.* **2021**, *63*, 1194–1200. [CrossRef]

45. Eyebe, G.A.; Bideau, B.; Boubekeur, N.; Loranger, É.; Domingue, F. Environmentally-friendly cellulose nanofibre sheets for humidity sensing in microwave frequencies. *Sens. Actuators B Chem.* **2017**, *245*, 484–492. [CrossRef]

46. Alipal, J.; Mohd Pu'ad, N.A.S.; Lee, T.C.; Nayan, N.H.M.; Sahari, N.; Basri, H.; Idris, M.I.; Abdullah, H.Z. A review of gelatin: Properties, sources, process, applications, and commercialisation. *Mater. Today Proc.* **2021**, *42*, 240–250. [CrossRef]

47. Khan, M.; Rehman, M.M.; Khan, S.A.; Saqib, M.; Kim, W.Y. Characterization and performance evaluation of fully biocompatible gelatin-based humidity sensor for health and environmental monitoring. *Front. Mater.* **2023**, *10*, 1233136. [CrossRef]

48. Shapardanis, S.; Hudpeth, M.; Kaya, T. Gelatin as a new humidity sensing material: Characterization and limitations. *AIP Adv.* **2014**, *4*, 127132. [CrossRef]

49. Gaaz, T.S.; Sulong, A.B.; Akhtar, M.N.; Kadhum, A.A.H.; Mohamad, A.B.; Al-Amiery, A.A. Properties and applications of polyvinyl alcohol, halloysite nanotubes and their nanocomposites. *Molecules* **2015**, *20*, 22833–22847. [CrossRef]

50. Gonzalez, J.S.; Burlaka, A.; Paz, J.; Salavagione, H.J.; Gonzalez, J.C.; Hernandez, R. Compact polyelectrolyte hydrogels of gelatin and chondroitin sulfate as ion's mobile media in sustainable all-solid state electrochemical devices. *Mater. Adv.* **2020**, *1*, 2526–2535. [CrossRef]

51. Vatanpour, V.; Teber, O.O.; Mehrabi, M.; Koyuncu, I. Polyvinyl alcohol-based separation membranes: A comprehensive review on fabrication techniques, applications and future prospective. *Mater. Today Chem.* **2023**, *28*, 101381. [CrossRef]

52. Kommareddy, S.; Shenoy, D.B.; Amiji, M.M. Gelatin nanoparticles and their biofunctionalization. In *Nanotechnologies for the Life Sciences: Online*; Wiley-VCH: Weinheim, Germany, 2007; pp. 330–352. [CrossRef]

53. Gelatin Handbook, Gelatin Manufacturers Institute of America Members 2019. Available online: http://www.gelatin-gmia.com/uploads/1/1/8/4/118450438/gmia_gelatin_manual_2019.pdf (accessed on 23 August 2024).

54. Su, L.; Vélez, P.; Casacuberta, P.; Muñoz-Enano, J.; Martín, F. Microwave humidity sensor for early detection of sweat and urine leakage. *Electronics* **2023**, *12*, 2276. [CrossRef]

55. Velez, P.; Su, L.; Grenier, K.; Mata-Contreras, J.; Dubuc, D.; Martin, F. Microwave microfluidic sensor based on a microstrip splitter/combiner configuration and split ring resonators (SRRs) for dielectric characterization of liquids. *IEEE Sens. J.* **2017**, *17*, 6589–6598. [CrossRef]

56. Yeo, J.; Lee, J.-I. High-sensitivity microwave sensor based on an interdigital-capacitor-shaped defected ground structure for permittivity characterization. *Sensors* **2019**, *19*, 498. [CrossRef] [PubMed]

57. Electromagnetic Simulation Solvers, CST Studio Suite. Available online: https://www.3ds.com/products-services/simulia/products/cst-studio-suite/solvers/ (accessed on 23 August 2024).

58. Hong, J.S.; Karyamapudi, B.M. A general circuit model for defected ground structures in planar transmission lines. *IEEE Microw. Wirel. Compon. Lett.* **2005**, *15*, 706–708. [CrossRef]

59. Saber, O.; Abu-Abdeen, M.; Aljaafari, A.; Mazher, J.; Ahmed, M.M.; BoNagma, O. New preparation approach, electrical and mechanical properties of poly(vinyl alcohol)-loaded graphene films. *J. Thermoplast. Compos. Mater.* **2021**, *34*, 1504–1522. [CrossRef]

60. Gareev, K.G.; Bagrets, V.S.; Golubkov, V.A.; Ivanitsa, M.G.; Khmelnitskiy, I.K.; Luchinin, V.V.; Mikhailova, O.N.; Testov, D.O. Synthesis and characterization of polyaniline-based composites for electromagnetic compatibility of electronic devices. *Electronics* **2020**, *9*, 734. [CrossRef]

61. Lu, D.; Maasch, M.; Penirschke, A.; Zheng, Y.; Damm, C.; Jakoby, R. Broadband permittivity characterization of polyvinyl-alcohol film for humidity sensing applications. *IEEE Trans. Microw. Theory Tech.* **2016**, *64*, 3255–3263. [CrossRef]